Tuning of plasmonic behaviours in coupled metallic nanotube arrays*

Fu Shao-Li(付少丽)[a], Li Hong-Jian(李宏建)[a)b)], Xie Su-Xia(谢素霞)[b)], Zhou Xin(周 昕)[b)], Xu Hai-Qing(徐海清)[a)], and Xia Hui(夏 辉)[a)†]

[a)] *College of Physics Science and Technology, Central South University, Changsha* 410083, *China*
[b)] *College of Materials Science and Engineering, Central South University, Changsha* 410083, *China*

(Received 19 May 2010; revised manuscript received 3 March 2011)

We theoretically investigate the influence of the shape of nanoholes on plasmonic behaviours in coupled elliptical metallic nanotube arrays by the finite-difference time-domain (FDTD) method. We study the structure in two cases: one for the array aligned along the minor axis and the other for the array aligned along the major axis. It is found that the optical properties and plasmonic effects can be tuned by the effective surface charges as a result of the variation in the minor axis length. Based on the localized nature of electric field distributions, we also clearly show that the presence of localized plasmon resonant modes originates from multipolar plasmon polaritons and a large magnitude of opposing surface charges build up in the gap between adjacent nanotubes.

Keywords: elliptical metallic nanotube array, surface plasmons, transmission spectrum, field distributions

PACS: 73.20.Mf, 78.68.+m, 78.30.–j **DOI:** 10.1088/1674-1056/20/8/087302

1. Introduction

Metallic nanostructures are of great interest because of their important applications in catalysis,[1] sensing,[2] surface-enhanced Raman scattering (SERS),[3] plasmon solar cells,[4,5] information storage,[6] photolithography,[7] and so on. They exhibit a rich variety of intriguing optical properties due to the interaction of the electromagnetic (EM) field with the free electrons of the metal. Such an excitation can occur at a metal–dielectric interface and is called a surface-plasmon polariton, or at a metallic nanoparticle and in this case it is termed a particle-plasmon polariton. The distinction accounts for the degree of localization of the plasmon. One of the most attractive features of plasmon excitation is the accompaniment with localized field enhancement and subwavelength focusing. There are several recent reviews of the physics and applications of surface plasmons.[8−10]

Nowadays, isolated metallic nanoparticles are usually chemically synthesized as colloidal suspensions and come in a variety of shapes and sizes. In the simple case of noble-metal nanospheres, the extinction spectrum is dominated by strong dipole plasmon resonances at visible frequencies. For elongated particles, the threefold degeneracy of these modes is lifted and one obtains a predominant nondegenerate longitudinal mode at lower frequencies as well as doubly degenerate transverse and other modes of mixed character at higher frequencies. These plasmon resonances can be tuned within a relatively broad range from infrared to visible frequencies by a proper choice of the geometrical characteristics, dielectric environment and material.[11−17] Therefore, elongated metallic nanoparticles, such as ellipsoids or cylinders, can be used as efficient and tunable optical antennas for manipulating light at the nanoscale. On the other hand, in metallic nanoparticle aggregates, interacting plasmons provide further possibilities to engineer the spectral response and tailor the light-matter interaction.

In contrast to a solid nanoparticle, the nanoshell is in itself a highly tunable metallic nanostructure consisting of a thin metallic shell around a dielectric core. It possesses several attractive features that make it interesting as a nanoscale optical component. These include tunable optical resonances depending on the

*Project supported by the Research Fund for the Doctoral Program of Higher Education of China (Grant No. 20100162110068), the Graduate Education Innovation Project of Central South University (Grant No. 2010ssxt010), and the Hunan Provincial Innovation Foundation for Postgraduate (Grant No. CX2009B029).

†Corresponding author. E-mail: xhui73@ mail.csu.edu.cn, lihj398@ yahoo.com.cn

© 2011 Chinese Physical Society and IOP Publishing Ltd

dimensions of the hollow interior and the thickness of the metallic shell, spanning a wide range of frequencies covering the visible and infrared regions of the optical spectrum.[18−21] This subwavelength structure can be used to manipulate light below the diffraction limit. For potential applications, it is highly desirable to develop new strategies to arrange hollow metal units into ordered structures and to allow control of their separation on a nanometer scale.

However, there is little understanding of the plasmonic properties of metallic nanotube arrays. In a recent paper,[22] the optical properties in a chain waveguide of an array of silver nanoshell with dielectric holes were studied and it was demonstrated that chain waveguides operated on resonant multipolar modes can provide longer propagation lengths, which is beyond what is maximally achieved by conventional solid particle chains. Recently, the near-field optical response of three-pair arrays of silver-shell nanocylinders, i.e., silver-nanotubes, has been studied. In this paper, we investigate theoretically the optical properties and surface plasmon effects of periodic arrays of elliptical metallic nanotubes with infinite lengths interacting with light by using the finite-difference time-domain (FDTD) method. This nanostructure combines the tunability introduced by the core/shell morphology with the tunability inherent in geometric anisotropy. We calculate the transmission spectra as a function of wavelength and study how the minor axis length affects the plasmonic behaviours of the metallic nanotube array. Furthermore, based on the instantaneous electric field distributions, we discuss the multipolar nature of plasmon resonances.

2. Model and theory

Figure 1 depicts schematically the model system that is composed of a one-dimensional array of nine identical elliptical metallic nanotubes with infinite length surrounded by air. The semimajor axis of the outer ellipse and the gap distance between adjacent nanotubes are set to be $a = 50$ nm and $d = 20$ nm, respectively, throughout our entire work. The semiminor axis of the outer ellipse is denoted as b. The wall thickness of the nanotube along major and minor axes is uniform and fixed at $T = 10$ nm, as shown in Fig. 1(a). Here, we focus on two cases: one for the array aligned along the minor axis (Fig. 1(b)) and the other for the array aligned along the major axis (Fig. 1(c)).

The interaction between light and Drude-type metal is generally described by time-dependent Maxwell equations, which are coupled to an equation describing the light-induced oscillation of quasifree-electrons in the metal:[23]

$$\begin{aligned} \boldsymbol{\nabla} \times \boldsymbol{E} &= -\mu_0 \frac{\partial \boldsymbol{H}}{\partial t}, \\ \boldsymbol{\nabla} \times \boldsymbol{H} &= \varepsilon_0 \frac{\partial \boldsymbol{E}}{\partial t} + \boldsymbol{J}, \\ \frac{\partial \boldsymbol{J}}{\partial t} &+ \gamma \boldsymbol{J} = \omega_{\mathrm{p}}^2 \varepsilon_0 E. \end{aligned} \tag{1}$$

where $\boldsymbol{E}$ is the electric field vector, $\boldsymbol{H}$ is the magnetic field vector, $\boldsymbol{J}$ is the electric current density corresponding to the metal polarization, and ω_{p} and γ are the metal plasma frequency and damping rate, respectively.

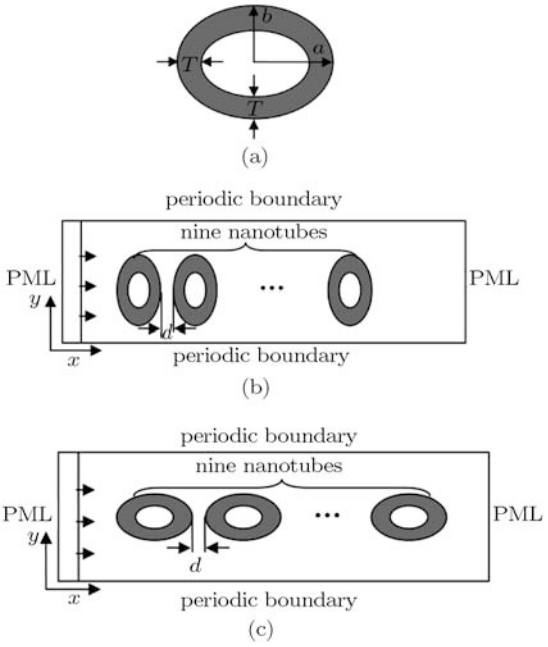


Fig. 1. (a) A schematic illustration of a single elliptical metallic nanotube with fixed outer long semiaxis $a = 50$ nm and variant outer minor semiaxis b in the x–y cross section, and the wall thickness in the major and minor direction is fixed at $T = 10$ nm. (b) The x–y cross section of the computational domain consisting of a single unit cell of the nine nanotube arrays arranged along the minor axis direction. (c) The x–y cross section of the computational domain consisting of a single unit cell of the nine nanotube arrays arranged along the major axis direction. In panels (b) and (c), the gap distance between adjacent nanotubes is fixed at $d = 20$ nm. Periodic boundary conditions are imposed on the surfaces along the y direction, while perfect matched layers (PML) are imposed on the surfaces along the x direction.

The transmission spectra and the distributions of the field intensities of the periodic elliptical gold nanotube arrays are simulated by using the FDTD

approach.[24] The FDTD method solves the time-dependent Maxwell's equations by discretizing space and time and it involves a relatively simple time-stepping algorithm. The frequency-dependent optical properties of the metallic nanotubes are approximated by the Drude model, which defines the dispersive permittivity as

$$\varepsilon(\omega) = 1 - \frac{\omega_{\rm p}^2}{\omega^2 + {\rm i}\omega\gamma_{\rm p}}. \tag{2}$$

In our simulation, the metallic nanotubes consist of gold, which is modeled with a bulk plasmon frequency $\omega_{\rm p} = 1.37 \times 10^{16}$ rad/s and an electron relaxation time $1/\gamma_{\rm p} = 24.5$ fs, describing the dissipative losses. These values are obtained by fitting the experimental results.[25] In our FDTD simulation, the spatial and temporal steps are set at $\Delta x = \Delta y = 1$ nm, and $\Delta t = \Delta x/2c$ (c is the velocity of light in vacuum). We simulated the structure with an FDTD cube of size $L_x \times L_y = 1240$ nm$\times$200 nm and infinity along the z direction. We excite the structure by an ultrashort linearly polarized pulse. The incident light polarizes along the y axis and irradiates the structure along the x direction in our work. Perfectly matched absorbing boundary conditions are applied at the left and right surfaces of the computational space along the x direction, whereas periodic boundary conditions are applied on other boundaries along the y direction. In our simulation, we calculate power $P(\omega)$. However, the power by itself is not very useful. In order to obtain the transmission spectrum, it needs to normalize. This is done by running the simulation twice: once with only the incident wave and no scattering structure, and once with the scattering structure, where the first calculation is used for normalization.

3. Results and discussion

We simulate the transmission spectra and the electric field distributions propagating through the elliptical gold nanotube array. A Gaussian-pulse source roughly proportional to $\exp(-{\rm i}\omega t - (t - t_0)^2/2w^2)$ is used in calculating the transmission spectra, where w is the frequency width used in the Gaussian-pulse source. In calculating the field distribution of the nanotube array the incidence is set to be a continuous wave source with a specified wavelength proportional to $\exp(-{\rm i}\omega t)$. For this hollow nanotube structure, the highly geometry-dependent plasmon response can be viewed as resulting from the hybridization of the solid elliptical nanocylinder plasmons associated with the outer surface of the tube and of the elliptical cavity plasmons associated with the inner surface.[26]

For comparison, in Fig. 2, we first investigate the transmission spectrum as a function of wavelength of the coupled metallic nanotube array with a circular cross section $a = b = 50$ nm. It is found that there exists a large photonic band gap in the visible light region at wavelengths from 411.8 nm to 582.9 nm. In the extraordinary optical transmission study of Ebbesen *et al.*,[27] the presence of gaps is due to the lifting of the degeneracy by surface plasmons (SPs) interacting with the lattice. In our work, the presence of gaps is also because of this. At wavelengths within a bandgap, the density of the SP modes is zero—no SP modes can be supported. We can also see that the resonant peaks on the left side of the band gap are very sharp, dense and irregular, whereas on the right side the resonant peaks are regular and the transmission gradually becomes higher and broader towards the longer wavelength.

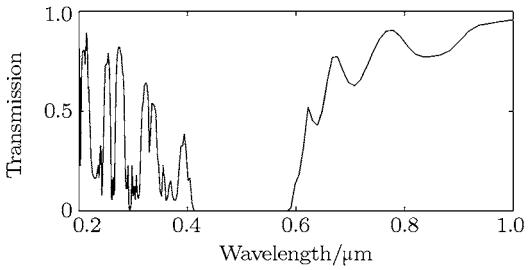


Fig. 2. Transmission spectrum as a function of wavelength for the circular metallic nanotube array, i.e., $a = b = 50$ nm.

In Fig. 3, we show the transmission spectra of the elliptical gold nanotube array, which is aligned along the minor axis as a function of wavelength with various semiminor axis lengths of (a) $b = 30$ nm, (b) $b = 35$ nm, and (c) $b = 40$ nm. When the minor axis length b of the nanotube is varied, we also proportionally change the lattice constant along the x direction. It is found that there appear two photonic band gaps, but the width of the left band gap is much smaller than that of the right one. Along with minor axis broadening, there appear new resonance peaks at the left band gap till the left band gap vanishes and the intensity of these resonance peaks are strengthened gradually. However, the intensity of the other resonance peaks changes little. Moreover, the right band gap's width increases as the length of the minor axis increases. These results show that SP excitation and confinement of light can be tuned by the length of the minor

axis. The plasmon frequency is determined by the ratio of the restoring force to the mass of the electron liquid. The mass is constant, and the restoring force originates from the Coulomb interaction of the surface charges on the opposite ends of the solid nanocylinder. As the solid elliptical nanocylinder deforms towards a circular nanocylinder, the magnitude of the effective surface charges on the tips of the nanocylinder increases and the spatial separation of the surface charges decreases. This increases the restoring force and redshifts the plasmon wavelength. For the ellptical cavity plasmons, the situations are reversed.[26] We observed that with an increase in the length of the minor axis, the resonance peaks at the right of the band gap show a slight redshift. This means that the solid plasmons dominate the plasmon resonance behaviours at longer wavelengths. We also observed that with an increase in the length of the minor axis, the resonance peaks at the shorter wavelength of the band gap change very little and this means that the solid plasmons and cavity plasmon collaborate with each other at shorter wavelengths.

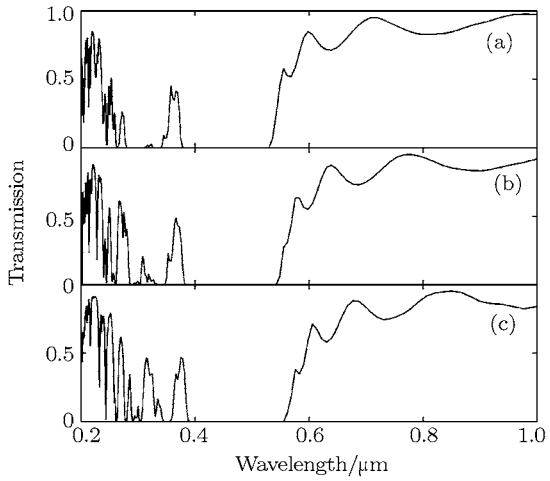


Fig. 3. Transmission spectra as a function of wavelength for the elliptical metallic nanotube array with different minor semiaxis lengths of (a) $b = 30$ nm, (b) $b = 35$ nm, and (c) $b = 40$ nm. The array is aligned along the direction of the minor axis.

Fundamental modes of the nanotube plasmons can also be illustrated with electric field distributions on the nanostructures. In Fig. 4, we draw the spatial distributions of the instantaneous electric field component E_x at steady state for the resonance modes closest to the band gap on the right in Fig. 3. The resonance wavelengths are (a) $\lambda = 0.5549$ μm, (b) $\lambda = 0.5756$ μm, and (c) $\lambda = 0.6058$ μm, respectively. Areas coloured white have positive field amplitude, while those coloured black have negative field amplitude. Such distributions can be used to discriminate between spectral features that correspond with collective dipole excitation and other physical resonances, or, in some cases, unphysical artifacts of the simulation. We can see that the distribution of the electric field component E_x is regular. Positive and negative fields alternately appear on the nanotubes. The existence of a dielectric gap means that the intertube interaction is highly capacitive in nature, and therefore a large magnitude of opposing surface charges build up in the gap between adjacent nanotubes. When the signs of the surface charges at the two sides of the gap are opposite, the electric fields in the gap are coupled together closely and intensified, which is just in analogy with a simple capacity device. In contrast, when they are uniform and repulsive to each other, the electric fields are decoupled and become very weak. It can be seen that as the length of the minor axis increases, spatial distribution of the electric field component E_x is more discontinuous due to the increased opposing surface charges in the gap. We can also see that the electric field is weakened by the increase in length of the minor axis. Moreover, the field perpendicular to the surface decays exponentially with distance from the surface. The field in this perpendicular direction is said to be evanescent or near field in nature and is a consequence of the bound, non-radiative nature of SPs, which prevents power from propagating away from the surface.

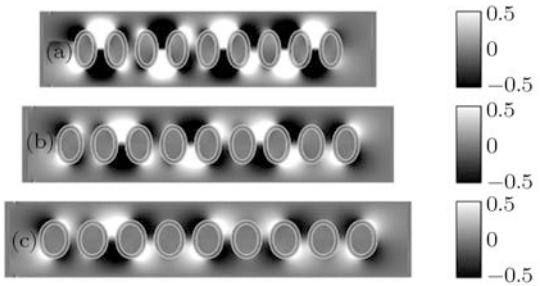


Fig. 4. The instantaneous electric field component E_x distribution at different resonance peak wavelengths closest to the longer wavelength photonic band edge in Fig. 3 for different lengths of minor semiaxis: (a) $b = 30$ nm, (b) $b = 35$ nm, and (c) $b = 40$ nm.

In Fig. 5, we calculate and compare the spatial distributions of the instantaneous electric field component E_x at steady state for the resonance modes in Fig. 3(b). The resonance peak wavelengths are (a) $\lambda = 0.3077$ μm, (b) $\lambda = 0.54623$ μm, and (c) $\lambda = 0.5756$ μm, respectively. For the multiparticle system, interactions between nanotubes allow a

greater degree freedom for the occurrence of plasmon resonances. Furthermore, it is well known that plasmonic nanoparticles may support higher-order localized resonances at optical frequencies, even when their total size is much smaller than the wavelength. We can see that there is a quadrupole field distribution for the plasmon mode in the array of the nanotubes in Fig. 5(c), hexpole in Fig. 5(b). However, composite higher order modes are excited at the shorter wavelength with narrower bandwidths in Fig. 5(a). In physical terms, the multipolar nature of nanotube plasmons is closely related to spherical harmonics, in which the expansion orders directly correspond to dipoles, quadrupoles, octopoles, and so forth. In addition, note that each nanotube should remain electrically neutral because the surface charges are all induced by polarizations. Moreover, the electric field distributions can also be observed inside the nanotube in Figs. 5(a) and 5(b). We consider that the longer wavelength peak (corresponding to Fig. 5(c)) may mainly originate from the elliptical nanocylinder plasmon coupling and the lower wavelength peaks (corresponding to the Figs. 5(a) and 5(b)) may mainly originate from the elliptical nanocylinder plasmons and elliptical cavity plasmon coupling.[26] This is consistent with the transmission in Fig. 3.

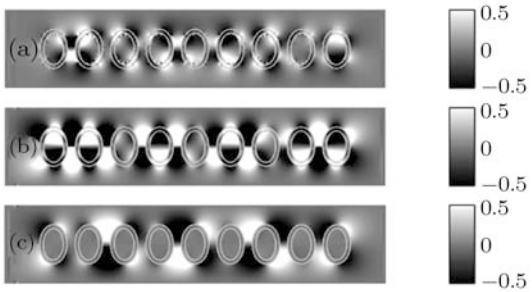


Fig. 5. The instantaneous electric field component E_x distributions at different resonance wavelengths: (a) $\lambda =$ 0.3077 μm, (b) $\lambda = 0.54623$ μm, and (c) $\lambda = 0.5756$ μm in Fig. 3(b).

We also investigated the plasmonic resonant coupling of the elliptical nanotube array, which is aligned along the major axis. In this situation, the incident light polarizes along the minor axis. Figure 6 illustrates the transmission spectra of this nanostructure as a function of wavelength. Different from Fig. 3, we can see that there is only one large photonic band gap, but the width of the resonance peaks near the band gap at the lower wavelength is very large and is narrowed with the increment of the length of the semiminor axis. We can also see that the intensity of the resonance peaks at the left of the band gap is weakened as the minor axis broadens. However, that at the right of the band gap changes little. In addition, as the length of the minor axis increases, the width of the band gap is broadened along both sides. The tunability of these plasmon energies of the array aligned along the major axis with its minor axis length can be understood qualitatively by using the same physical argument invoked in the discussion of the plasmons of the nanotube aligned along the minor axis. As the elliptical solid nanocylinder is deformed towards a circular nanocylinder, the effective surface charges increase and their separation decreases, leading to a bigger restoring force and a redshift of the plasmon wavelengths. For the elliptical cavity plasmons, the situations are reversed.[26]

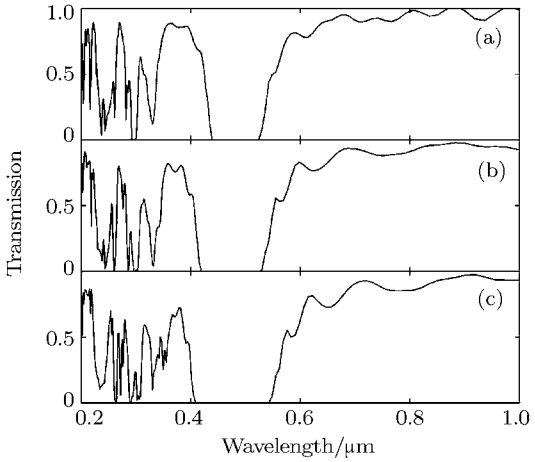


Fig. 6. Transmission spectra as a function of wavelength for the oblate metallic nanotube array with different lengths of minor semiaxis: (a) $b = 30$ nm, (b) $b = 35$ nm, (c) $b = 40$ nm. The array is aligned along the direction of the major axis.

Figure 7 shows the spatial distributions of the instantaneous electric field component E_x at steady state closest to the band gap with various lengths of semiminor axis: (a) $b = 30$ nm, (b) $b = 35$ nm, and (c) $b = 40$ nm. The resonance peak wavelengths are (a) $\lambda = 0.5484$ μm, (b) $\lambda = 0.5549$ μm, and (c) $\lambda = 0.5756$ μm, respectively. It can be seen that the distributions of the electric field component E_x are all regular in Figs. 7(a)–7(c) and those in Figs. 7(a) and 7(c) are almost the same. At $\lambda = 0.5484$ μm and $\lambda = 0.5756$ μm, the electric field of the first nanotube is isolated but in Fig. 7(b) $\lambda = 0.5549$ μm the electric field enhancement is mostly concentrated at the gap of every other three nanotubes. For both cases, we can see that the plasmon energies converge to the

circular nanotube plasmon energies when the length of the minor axis equals the length of the major axis.

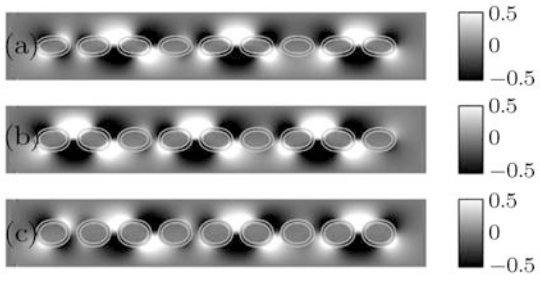


Fig. 7. The instantaneous electric field component E_x distribution at different resonance peak wavelengths closest to the longer wavelength photonic band edge in Fig. 6 for different lengths of minor semiaxis: (a) $b = 30$ nm, (b) $b = 35$ nm, and (c) $b = 40$ nm.

4. Conclusion

In conclusion, we have used the FDTD method to calculate the transmission spectra and the field distributions of the elliptical gold nanotube arrays. We first studied the nanotube array of circular cross section. It is found that there exists a large photonic band gap in the transmission spectra. Then we investigated the elliptical nanotube and focused on two cases: one for the array aligned along the minor axis and the other for the array aligned along the major axis. It was demonstrated that the plasmonic behaviours are strongly dependent on the length of the minor axis. For the array aligned along the minor axis, there exist two photonic band gaps, and the band gap at the lower wavelength vanishes as the new resonance peaks occur with the broadening minor axis. But there is only one band gap when the array is aligned along the major axis. Based on the field distributions, we show that there is a quadrupole field distribution for the plasmon mode on the right of the band gap, but composite higher order modes are excited at the shorter wavelengths on the left of the band gap. We attribute this phenomenon to the increased effective surface charges with the broadening minor axis. The simulation results of this metallic nanotube array may be suitable for the design of surface plasmon resonance processing or nano-photonic device.

References

[1] Lieber C M 1998 *Solid State Commun.* **107** 607
[2] Jain P K and El-Sayed M A 2008 *Nano Lett.* **8** 4347
[3] Banholzer M J, Millstone J E, Qin L and Mirkin C A 2008 *Chem. Soc. Rev.* **37** 885
[4] Hagglund C, Zach M, Petersson G and Kasemo B 2008 *Appl. Phys. Lett.* **92** 053110
[5] Wang J F, Li H J, Zhou Z Y, Li X Y, Liu J and Yang H Y 2010 *Chin. Phys.* B **19** 117310
[6] Murray C B, Sun S, Doyle H and Betley T 2001 *Mater. Res. Soc. Bull.* **26** 985
[7] Li H H, Chen J and Wang Q K 2010 *Chin. Phys.* B **19** 114203
[8] Maier S A 2007 *Plasmonics: Fundamentals and Applications* (Dordrecht: Springer)
[9] Brongersma M L and Kik P G 2007 *Surface Plasmon Nanophotonics* (Dordrecht: Springer)
[10] Shalaev V M and Kawata S 2007 *Nanophotonics with Surface Plasmons* (Oxford: Elsevier)
[11] Khlebtsov B N and Khlebtsov N G 2007 *J. Phys. Chem.* C **111** 11516
[12] Imura K, Nagahara T and Okamoto H 2005 *J. Chem. Phys.* **122** 154701
[13] Huang Q, Zhang X D, Zhang H, Xiong S Z, Geng W D, Geng X H and Zhao Y 2010 *Chin. Phys.* B **19** 047304
[14] Guo Y N, Xue W R and Zhang W M 2009 *Acta Phys. Sin.* **58** 4168 (in Chinese)
[15] Prescott S W and Mulvaney P 2006 *J. Appl. Phys.* **99** 123504
[16] Liu M, Guyot-Sionnest P, Lee T W and Gray S K 2007 *Phys. Rev.* B **76** 235428
[17] Nehl C L and Hafner J H 2008 *J. Mater. Chem.* **18** 2415
[18] Prodan E, Nordlander P and Halas N J 2003 *Nano Lett.* **3** 1411
[19] Teperik T V, Popov V V and G de Abajo F J 2004 *Phys. Rev.* B **69** 155402
[20] Oubre C and Nordlander P 2004 *J. Phys. Chem.* B **108** 11740
[21] Zhang H X, Gu Y and Gong Q H 2008 *Chin. Phys.* B **17** 2567
[22] Chau Y F, Yeh H H, Liu C Y and Tsai D P 2010 *Opt. Commun.* **283** 3189
[23] Chau Y F, Yeh H H and Tsai D P 2009 *Phys. Plasmas* **16** 022303
[24] Taflove A and Hagness S C 2000 *Computational Electrodynamics: The Finite-Difference Time-Domain Method*, 2nd edn. (Boston: Artech House)
[25] Palik E D 1985 *Handbook of Optical Constants in Solids* (Boston: Academic)
[26] Brandl D W and Nordlander P 2007 *J. Chem. Phys.* **126** 144708
[27] Ebbesen T W, Lezec H J, Ghaemi H F, Thio T and Wolff P A 1998 *Nature* **391** 167